Charge disproportionation of mixed-valent Cr triggered by Bi lone-pair effect in the *A*-site-ordered perovskite $BiCu_3Cr_4O_{12}$

Martin Etter,[1,*] Masahiko Isobe,[1,†] Hiroya Sakurai,[2] Alexander Yaresko,[1] Robert E. Dinnebier,[1] and Hidenori Takagi[1,3,‡]
[1]*Max Planck Institute for Solid State Research, D-70569 Stuttgart, Germany*
[2]*National Institute for Materials Science (NIMS), Tsukuba, Ibaraki 305-0044, Japan*
[3]*Department of Physics, University of Tokyo, Bunkyo-ku, Tokyo 133-0022, Japan*

(Received 8 January 2018; revised manuscript received 17 April 2018; published 8 May 2018)

A new *A*-site-ordered perovskite $BiCu_3Cr_4O_{12}$ is synthesized under a high pressure of 7.7 GPa. A phase transition from a paramagnetic metal to a ferrimagnetic metal is observed at $T_c = 190$ K accompanied with a structural change from cubic to monoclinic. Structural analysis of the low-temperature monoclinic phase reveals that this transition represents a charge disproportionation of $Cr^{3.75+}$ into Cr^{4+} and $Cr^{3.5+}$. We argue that the asymmetric displacement of Bi caused by a lone-pair effect triggers the formation of a dimeric $Cr^{4+}{}_2O_5$ unit and leads to an ordering of Cr^{4+} and $Cr^{3.5+}$ below the transition.

DOI: 10.1103/PhysRevB.97.195111

I. INTRODUCTION

Mixed-valent oxides, with an admixture of two different valence states of transition metal ions such as 3+ and 4+, have been a major arena in the exploration of novel electronic phases in correlated transition metal oxides. A charge homogeneous metallic state of mixed-valent oxides often shows a transition to a charge inhomogeneous state at low temperatures called charge disproportionation (charge ordering), where a spatially ordered state of ions with two different valence states is realized. The coupling of charge with spin and orbital degrees of freedom and/or the transfer of charge between the two different constituent elements can give rise to a rich variety of complicated ordering pattern of charges, almost degenerate and competing with each other, that are intimately coupled with spins and orbitals [1–8].

The *A*-site-ordered perovskites with a chemical formula of $RECu_3B_4O_{12}$ are one of the prototypical mixed-valent oxides families. When trivalent rare earth ions occupy the RE site and Cu is divalent, the formal valence of the B cation is +3.75: a mixed valence state with 1:3 ratio of B^{+3} and B^{+4} ions. $RECu_3B_4O_{12}$, where RE is trivalent rare earth ions and B is 3*d* transition metals (V, Cr, Mn, Fe, and Co), have been studied extensively. Three kinds of ground states were found: a homogeneous mixed-valent state, a charge transferred state between Cu and B, and a charge disproportionate state of B. All the V and Mn compounds belong to the first group and do not show any structural transition indicative of charge disproportionation or transfer, and they remain metallic. While the V compounds remain paramagnetic down to the lowest temperature [9], the Mn compounds show a ferrimagnetic transition [10]. All the Cr and Co compounds reported so far [11–15] and Fe compounds with a large ionic radius of RE^{3+} ions [16] are categorized into the second group, where a transition to all B^{3+} state, namely $RE^{3+}Cu^{3+}{}_3B^{3+}{}_4O_{12}$, is realized associated with a charge transfer between Cu and B. Most of them show an antiferromagnetic ordering at the charge transfer transition. While Co compounds all become insulators in the charge transferred state, Cr compounds remain poorly metallic down to the lowest temperature [11–14]. Charge disproportionate states are surprisingly rare in $RECu_3B_4O_{12}$; only several Fe compounds with small RE^{3+} ions show a charge disproportionation into 5:3 ratio of Fe^{3+} and Fe^{5+} and turn into ferrimagnetic insulators below the transition temperature [16].

In this paper, we report that $BiCu_3Cr_4O_{12}$ with RE = Bi^{3+} instead of trivalent rare earth ions behaves very differently from the other $RECu_3Cr_4O_{12}$ and shows a charge disproportionation of Cr. This apparently violates the systematic trend of the ground states among $RECu_3B_4O_{12}$ family. To our knowledge, a charge disproportionation transition is observed for the first time not only in the $RECu_3Cr_4O_{12}$ family but also in mixed-valent Cr compounds in general. We argue that the formation of an asymmetric lone-pair state of Bi^{3+} triggers the unusual charge disproportionation of Cr.

II. EXPERIMENT

A belt-type high-pressure apparatus was used for the synthesis. A polycrystalline sample of $BiCu_3Cr_4O_{12}$ was prepared from a stoichiometric mixture of Bi_2O_3, CuO, Cr_2O_3, and CrO_2. The mixture was sealed in a gold capsule and heated at 1473 K for 2 h under a high pressure of 7.7 GPa. Then the capsule was quenched to room temperature, where the pressure was gradually released. Black fragile pellets were obtained.

Synchrotron x-ray powder diffraction on the obtained sample was conducted at beamline X17B1 at the National Synchrotron Light Source of Brookhaven National Laboratory. The powder patterns in Debye-Scherrer mode were collected at a wavelength of $\lambda = 0.1839$ Å (67.42 keV) with a Si(311) sagittal focusing double Laue crystal monochromator and a

*Present address: Deutsches Elektronen-Synchrotron (DESY), D-22607 Hamburg, Germany.
†m.isobe@fkf.mpg.de
‡h.takagi@fkf.mpg.de

Perkin Elmer image plate detector. The measured sample was cooled/heated with an Oxford cryostream 700 cold gas blower. The collected two-dimensional Debye-Scherrer rings were subsequently integrated with the program FIT2D [17] to one-dimensional powder diffraction patterns. The parameters for integration were determined from a LaB_6 reference sample. Using the software TOPAS [18], sequential Rietveld refinements were carried out, applying the fundamental parameter method [19] for peak modeling and Chebyshev polynomials for modeling the background. Symmetry modes for the refinement of atomic coordinates were determined by the ISODISTORT software [20].

Magnetic properties were measured by a SQUID magnetometer (MPMS, Quantum Design) in a temperature range of 5–300 K and in a magnetic field range of 0–5 T. The DC electrical resistivity was measured in a temperature range of 2–300 K using a Physical Property Measurement System (Quantum Design). The sample dimensions for the resistivity measurements were $0.5 \times 0.5 \times 1.0\,\mathrm{mm}^3$.

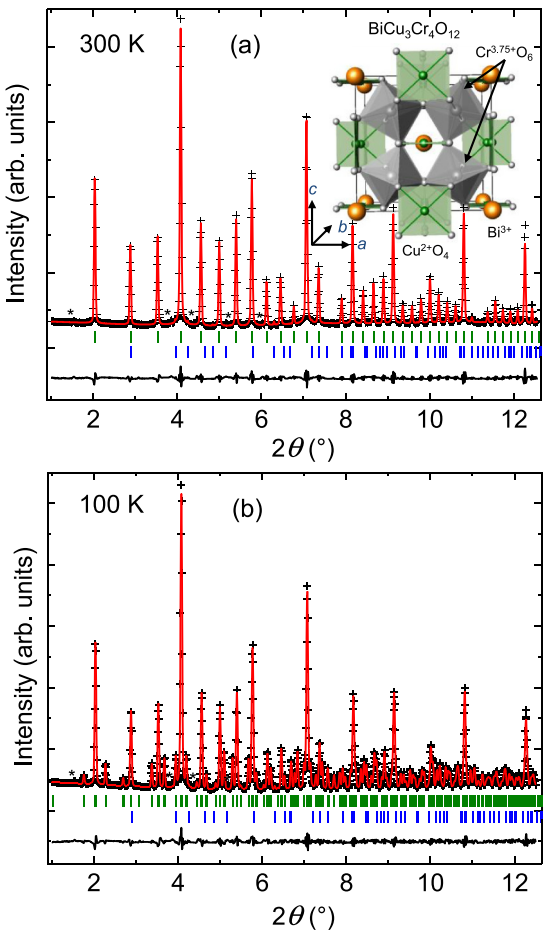

FIG. 1. Rietveld refinement of synchrotron x-ray powder diffraction data. The green and blue ticks indicate the position of the Bragg peaks of the $Im\bar{3}$ the structure at 300 K (a) and the $C2/m$ structure at 100 K, and of the Cr_2O_3 impurity (top and bottom). The black line indicates the difference between the observed and calculated profile. Very small peaks from an unknown phase are present as marked by asterisks. Projection of the cubic crystal structure of $BiCu_3Cr_4O_{12}$ at 300 K as shown in the inset to (a).

Electronic band structure calculations were performed within the local density approximation (LDA) using the relativistic PY LMTO computer code [21].

III. RESULTS AND DISCUSSION

$BiCu_3Cr_4O_{12}$ crystallizes at room temperature in space group $Im\bar{3}$ with cubic perovskite lattice parameter of $2a_p \times 2a_p \times 2a_p$ ($2a_p = 7.3028(1)$ Å) [the inset of Fig. 1(a)], isostructural to the other A-site-ordered perovskites. A 1:3 ratio of Bi and Cu occupy the A site of simple perovskite and order three-dimensionally to form a body-centered sublattice of Bi.

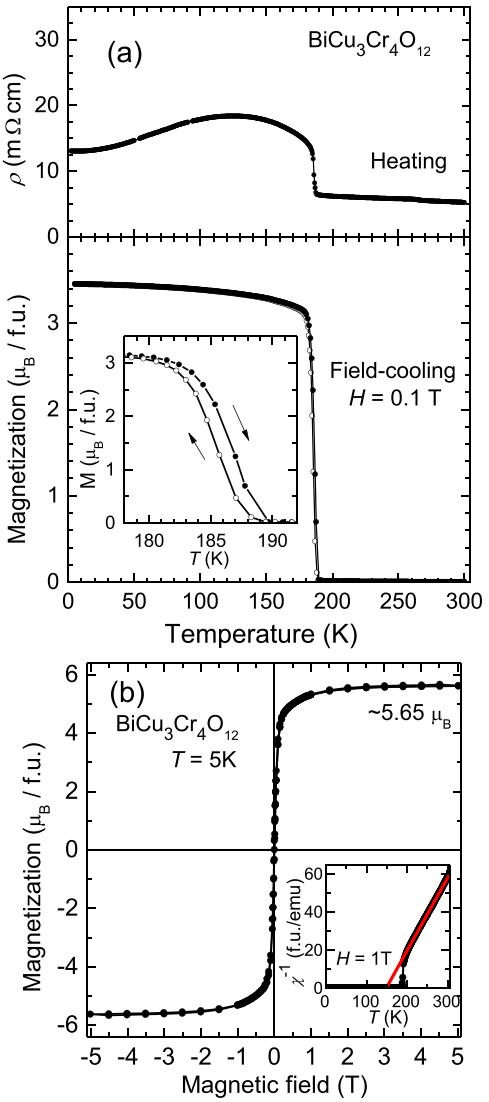

FIG. 2. (a) Temperature dependence of the electric resistivity $\rho(T)$ and the magnetization $M(T)$ under a magnetic field $H = 0.1$ T for $BiCu_3Cr_4O_{12}$. A discontinuous change at around 190 K is clearly observed both in $\rho(T)$ and $M(T)$. A thermal hysteresis in $M(T)$ is displayed in the inset to (a). (b) Magnetization curve $M(H)$ of $BiCu_3Cr_4O_{12}$ at 5 K, showing a saturation moment of $M_S = 5.65\,\mu_B$/f.u. In the paramagnetic regime, the inverse susceptibility can be fitted with a Curie-Weiss law with a Curie constant of $C = 2.61$ emuK/mol ($4.6\,\mu_B$/f.u.) and a Curie-Weiss temperature of $\theta_{CW} = +149$ K as shown in the inset.

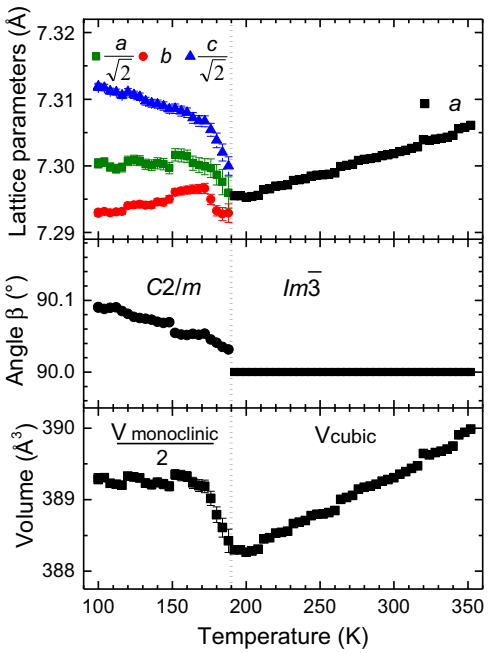

FIG. 3. Temperature dependence of the lattice parameters, the monoclinic angle, and the volume on heating.

The cation ordering gives rise to a displacement of oxygens. Cu takes a square-planar-coordination with oxygens, distinct from the 12-fold coordination in the original perovskite structure, which is accompanied with the tilting of CrO_6 octahedra. A Rietveld plot of the room temperature structure is presented in Fig 1(a). The detailed structure parameters can be found in Supplemental Material Table I [22]. The bond-valence sum analysis [23] confirms that, at room temperature, the calculated valences of Bi (+3.11), Cu (+1.98), and Cr (+3.60) are very close to their ideal values of +3.0, +2.0, and +3.75, respectively. This is fully consistent with the mixed-valence state with a ratio of 1:3 for Cr^{3+} and Cr^{4+} ions.

The resistivity $\rho(T)$ and the magnetization $M(T)$ measurements of $BiCu_3Cr_4O_{12}$ reveals the presence of a first-order transition from a paramagnetic metal to a ferrimagnetic metal at 190 K.

The $\rho(T)$ in Fig. 2(a) shows almost temperature-independent behavior at room temperature. With decreasing temperature, a discontinuous jump of $\rho(T)$ is observed at $T_c = 190$ K, followed by a poorly metallic behavior. The resistivity jump is accompanied with the emergence of a ferromagnetic moment in $M(T)$ in Fig. 2(a). The magnetization curve $M(H)$ at 5K in Fig. 2(b) indicates a saturation moment $M_s = 5.65\,\mu_B$/f.u., very close to the expected value of $6\,\mu_B$/f.u. for a ferrimagnetic ordering of the Cu^{2+} ($S = 1/2$, $\downarrow$) and $Cr^{3.75+}$ (Cr^{3+} : $S = 3/2$, $\uparrow$; Cr^{4+} : $S = 1$, $\uparrow$) spins. A small thermal hysteresis in $M(T)$ is found around T_c as shown in the inset to Fig. 2(a), indicating that the transition is first order. The temperature dependence of susceptibility $M(T)/H$ above T_c can be fitted with the Curie-Weiss law, yielding an effective moment $p_{eff} = 4.6\,\mu_B$/f.u. and a Curie-Weiss temperature $\theta_{CW} = +149$ K, indicative of a predominantly ferromagnetic interaction [the inset of Fig. 2(b)]. The occurrence of ferrimagnetic ordering contrasts with the other $RECu_3Cr_4O_{12}$, where antiferromagnetic ordering takes place at the charge-transfer transition [7–9], suggesting that the nature of the low temperature transition in $BiCu_3Cr_4O_{12}$ is distinct from those of the other $RECu_3Cr_4O_{12}$.

The x-ray diffraction measurements at low temperatures indicate that the transition at 190K is accompanied with a structural change from cubic to monoclinic with space group $C2/m$. The unit cell in the monoclinic phase is doubled ($2\sqrt{2}a_p \times 2a_p \times 2\sqrt{2}a_p$) as compared with the high temperature cubic phase. A Rietveld plot of the 100 K is shown in Fig. 1(b). The refined structural parameters at 100 K are listed in Supplemental Material Table II [22]. The temperature

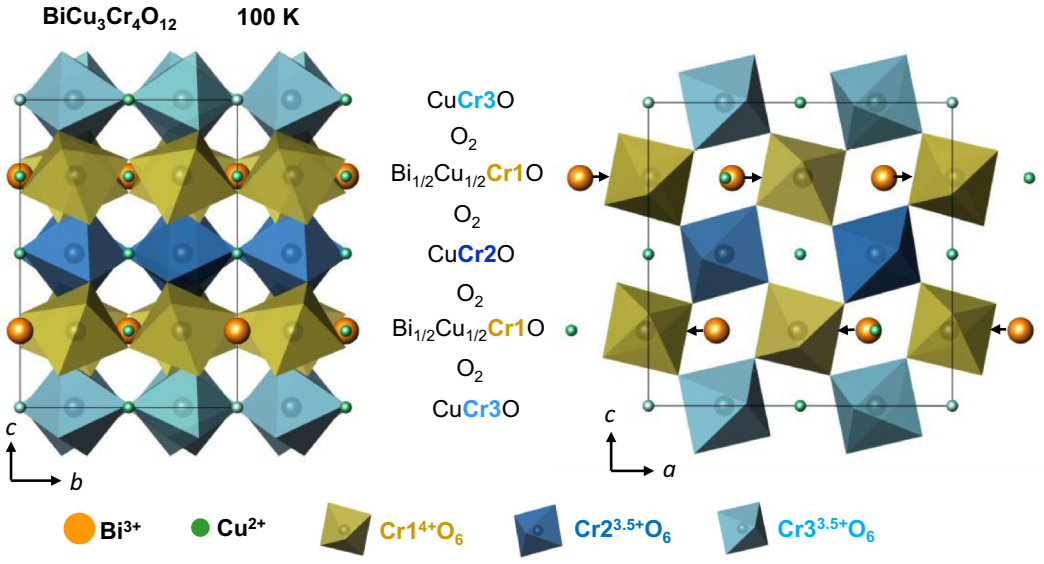

FIG. 4. Projection of the monoclinic crystal structure of $BiCu_3Cr_4O_{12}$ at 100 K. The view is along the a^* axis and the b^* axis. The three inequivalent Cr sites are indicated by the color of the CrO_6 octahedra (yellow = Cr1, blue = Cr2, light blue = Cr3). We assign the valences of Cr1, Cr2 and Cr3 to 4+, 3.5+ and 3.5+ respectively. The black arrows indicate the shift of Bi atoms.

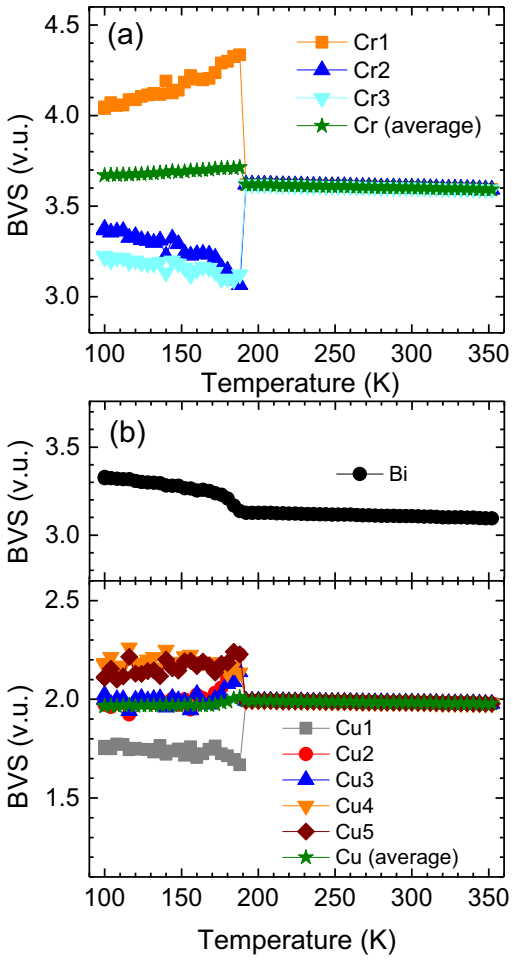

FIG. 5. Temperature dependence of bond valence sums (BVS) of Cr, Bi, and Cu for $BiCu_3Cr_4O_{12}$.

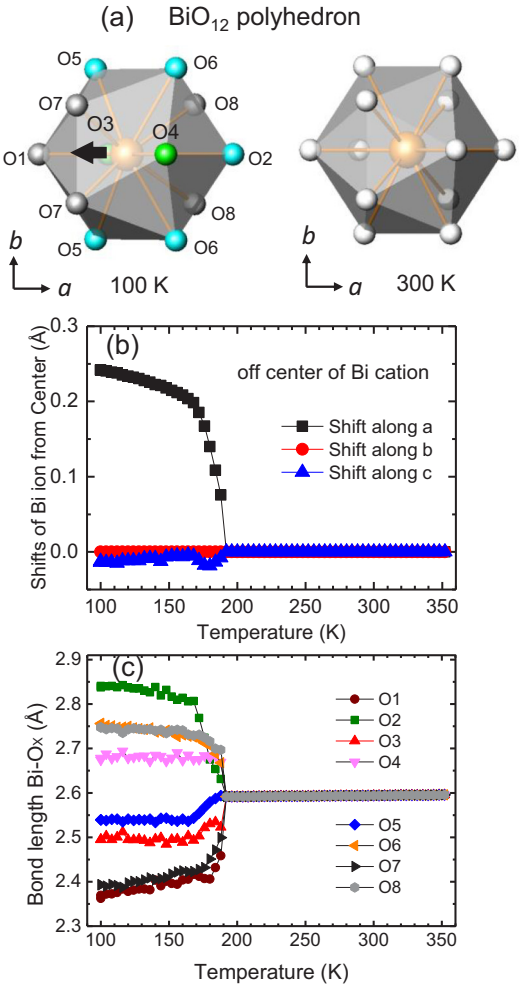

FIG. 6. (a) Projection of the BiO_{12} polyhedron at 100 and 300 K. (b) Temperature dependence of the shift of Bi from center of O_{12} polyhedron surrounding Bi in $BiCu_3Cr_4O_{12}$. (c) Temperature dependence of the bond-lengths of Bi-O_X in the BiO_{12} of $BiCu_3Cr_4O_{12}$. The definition of O1, O2, O5, O6, O7, and O8 is the same as in Fig. 7.

dependence of lattice parameters is shown in Fig. 3. The discontinuous jump of the lattice parameters at $T_c = 190$ K is consistent with the first-order transition. The distortion of the CrO_6 octahedron and the Cu and Bi positions in the low-temperature monoclinic phase are visualized in Fig. 4. The number of unique crystallographic sites for Cr increases from one to three. The three inequivalent Cr sites, Cr1 (yellow), Cr2 (blue), and Cr3 (light blue), respectively, form three kinds of corner-shared chains of CrO_6 octahedra running along the *b* axis. In the *ac* plane perpendicular to the chains, they form stripes running along the *a* axis and order along the *c* axis as Cr3-Cr1-Cr2-Cr1-Cr3 stripes. The ratio of Cr1, Cr2, and Cr3 sites is therefore 2:1:1. There remains only one unique Bi-site but the number of Cu sites increases from one to five. The full crystal structure can be described as an alternative stacking along the *c* axis of (CuCr3O)-O_2-($Bi_{1/2}Cu_{1/2}$Cr1O)-O_2-(CuCr2O)-O_2-($Bi_{1/2}Cu_{1/2}$Cr1O)-O_2-(CuCr3O) layers.

The results of bond-valence sum calculations are summarized in Fig. 5. The valence state of Cr shows a discontinuous change across $T_c = 190$ K. The three inequivalent Cr sites below T_c, Cr1, Cr2, and Cr3, with the ratio of 2:1:1 change their valence from +3.6 at 300 K to +4.03, +3.36 and +3.22, respectively, at 100 K. The valence state below T_c is close to +4.0, +3.5, and +3.5, though an appreciable temperature dependence of Cr valence state is clearly visible. The average valence of 2:1:1 ratio of Cr1, Cr2, and Cr3, however, is 3.66 and does not change appreciably at T_c. The valence of Bi increases only slightly from 3.11 at 300 K to 3.30 at 100 K. The valences of Cu are slightly different among the five crystallographic sites but the average remains around +1.98. These observations are indicative of the absence of charge transfer between Cu and Cr as observed in $RECu_3Cr_4O_{12}$. The disproportionation of charge takes place essentially within Cr, electrons being transferred from Cr1 to Cr2 and Cr3. This situation may be viewed as a charge disproportionation of $Cr^{3.75+}$ into 1:1 ratio of Cr^{4+} and $Cr^{3.5+}$ or, to be more precise, $Cr^{(4+\delta)+}$ and $Cr^{(3.5-\delta)+}$ with a small and temperature-dependent parameter δ. We conclude therefore that charge disproportionation of Cr occurs in $BiCu_3Cr_4O_{12}$, which is unique among Cr oxides. We consider that after the charge disproportionation the resistivity still shows a poorly metallic behavior because Cr^{4+} and $Cr^{3.5+}$ oxides can be metallic.

In the distorted structure below the transition, an asymmetric displacement of Bi can be seen along the *a* axis from the

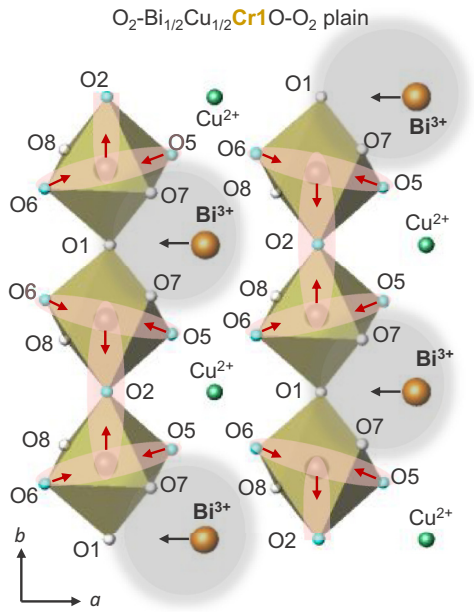

FIG. 7. The O_2-$Bi_{1/2}Cu_{1/2}$Cr1O-O_2 plane perpendicular to the c axis in the low temperature monoclinic phase of $BiCu_3Cr_4O_{12}$. The interaction between $Cr1O_6$ chains running along b axis and the lone-pair Bi ions can be seen. The shifts of Bi, Cr, and O atoms from the high temperature cubic structure are indicated by the arrows.

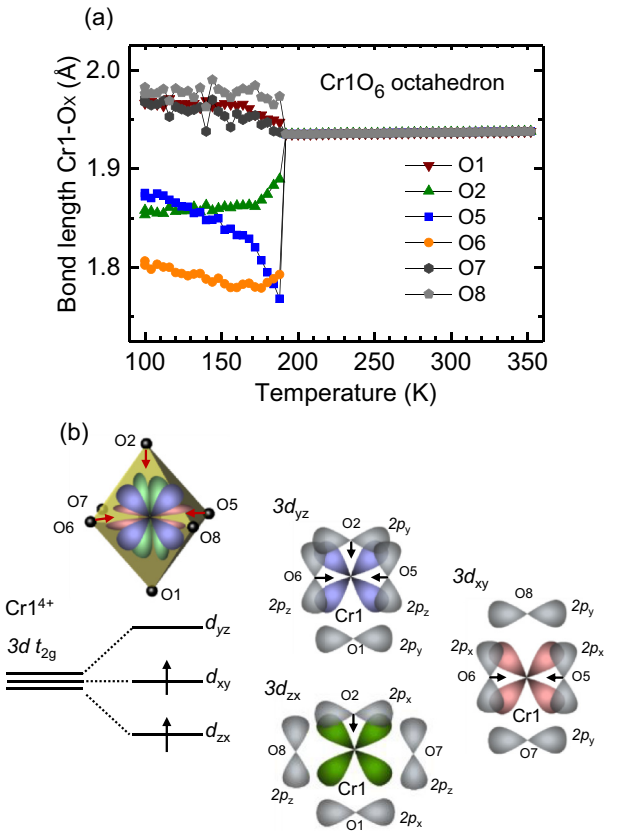

FIG. 8. (a) Temperature dependence of Cr1-O bond lengths for six oxygens O1, O2, O5, O6, O7, and O8 in $Cr1O_6$ octahedron shown in Fig. 7. (b) Top left: Projection of the $Cr1O_6$ octahedron with Cr $3d$ t_{2g} orbitals. xy, yz, and zx orbitals are colored by red, blue, and green, respectively. Below: Orbital splitting of Cr1 t_{2g} orbitals expected from the distortion of $Cr1O_6$ octahedron. Right: Illustration of the interactions between t_{2g} orbitals of Cr1 and $2p$ orbitals of oxygens in $Cr1O_6$ with the distortion below the phase transition.

center of the BiO_{12} polyhedron in Figs. 4 and 6 (indicated by arrows). The local distortion is the same type as in the ferroelectric state of perovskites with A-site Bi, which can be understood as the formation of Bi lone pair [24]. By mixing up empty Bi $6p$ states associated with the asymmetric shift, the filled Bi $6s$-O$2p$ states can lower their energy.

We argue that the asymmetric displacement often observed for Bi^{3+} triggers the charge disproportionation of Cr in $BiCu_3Cr_4O_{12}$. The CrO_6 octahedra share common oxygen atoms with the neighboring BiO_{12} polyhedra and therefore the displacement of Bi and the resultant distortion of the oxygen polyhedra modifies the local environment of Cr. Indeed, as shown in Figs. 6 –8, the asymmetric shift of Bi is toward the Cr1 chains where the high valence state of Cr^{4+} is realized. $Cr1O_6$ octahedra have six oxygen sites, O1, O2, O5, O6, O7, and O8. Above T_c, CrO_6 octahedra are regular with all equal Cr-O bond lengths, 1.938 Å at 300 K. Below T_c, Bi approaches O1 and O7 and makes stronger bonds with them as shown in Fig. 7. A small increase of the Cr bond lengths with oxygens forming Bi bonds, Cr1-O1 and Cr1-O7, is observed as shown in Fig. 8(a), as well as those for Cr1-O8 (O8; diagonal of O7). In sharp contrast, Cr1 and the rest of oxygens, O5, O6, and O2, come close to each other and appear to form a Cr_2O_5 [(O6Cr1O5)O2(O6Cr1O5)] molecular units with extremely short Cr1-O5, Cr1-O6, and Cr1-O2 bonds, 1.875 Å, 1.806 Å, and 1.850 Å at 100 K as displayed in Figs. 7 and 8(a). This apparently mirrors the strong Bi-O1 and Bi-O2 asymmetric bonding associated with the lone-pair formation. We argue that the formation of the three very short bonds gives rise to the high valence 4+ state for Cr1 in the valence bond sum calculation. As shown schematically in Fig. 8(b), the three short bonds stabilize d_{zx} and destabilize d_{yz} through the ligand field splitting caused by the p-d hybridization. The destabilization of the d_{yz} state prefers empty d_{yz} state and, hence, d^2 Cr^{4+}. Note that $Cr2O_6$ and $Cr3O_6$ are less distorted (Supplemental Material Fig. 1 [22]) and their degenerate $3d$ t_{2g} levels do not split as much as in $Cr1O_6$ octahedron, which stabilizes the $Cr^{3.5+}$ state with 2.5 d electrons for Cr2 and Cr3.

The emergence of a stereo-active Bi lone-pair in $BiCu_3Cr_4O_{12}$ is fully supported by the results of LDA band calculations. Total and partial densities of states (DOS) of $BiCu_3Cr_4O_{12}$ in the cubic and the monoclinic phases are shown in Fig. 9, which are calculated by using experimentally determined atomic positions at 300 K and at 100 K, respectively. Bi $6s$, O$2p$, Cr $3d$ t_{2g}, Bi $6p_{1/2}$, Cr $3d$ e_g, and $6p_{3/2}$ bands are centered around −11.5 eV, −5 eV, 0 eV, 2 eV, 3 eV, and 4.5 eV, respectively. Bi partial DOS shows a substantial contribution of the Bi $6s$ states to the O $2p$ band between −5 and −3 eV which can be ascribed to Bi $6s$-O $2p$ antibonding states. The contribution of Bi $6p$ states near the bottom of O$2p$ band and the appreciable O p DOS in the Bi $6p_{1/2}$ and $6p_{3/2}$ bands evidence rather strong Bi p-O p hybridization, which helps in stabilizing the structure. Whereas in the high temperature cubic structure Bi $6p$ states do not admix to the antibonding O $2p$-Bi $6s$ bands, in the low-temperature monoclinic phase

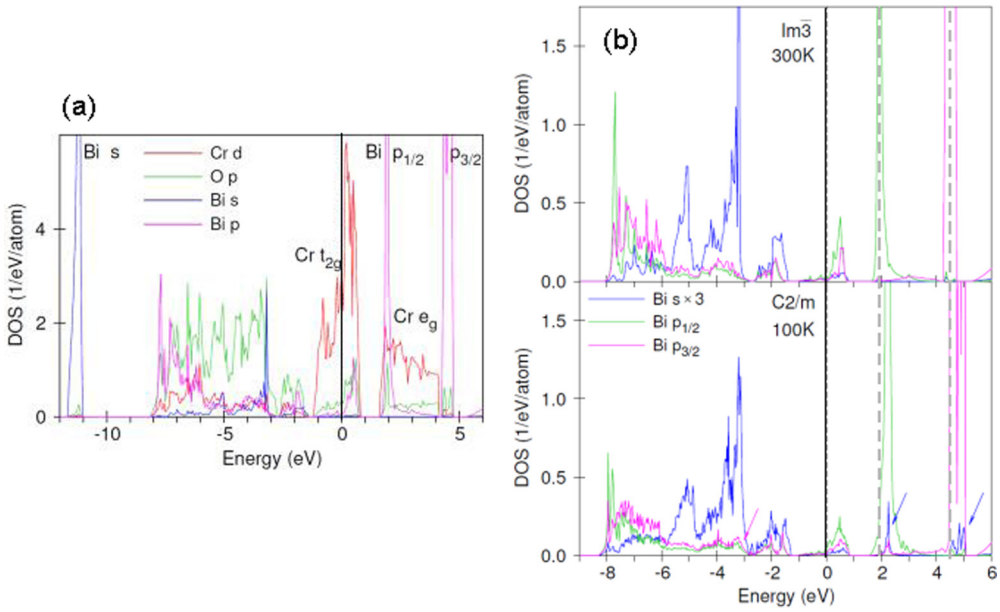

FIG. 9. (a) Partial densities of states (DOS) of Cr d, O p, Bi s, and Bi p calculated for the $Im\bar{3}$ structure (300 K) of $BiCu_3Cr_4O_{12}$. Bi $6s$, O$2p$, Cr $3d$ t_{2g}, Bi $6p_{1/2}$, Cr $3d$ e_g, and $6p_{3/2}$ bands are centered around -11.5 eV, -5 eV, 0 eV, 2 eV, 3 eV, and 4.5 eV, respectively. (b) Comparison between the calculated DOS for the $Im\bar{3}$ (300 K) and the $C2/m$ (100 K) structure of $BiCu_3Cr_4O_{12}$. Bi s contribution in the Bi $6p$ bands and Bi p contribution for O $2p$-Bi $6s$ antibonding can be identified only in the distorted $C2/m$ (100 K) structure, which are indicated by arrows. $C2/m$ (100 K) phase, B $6p$ bands shift to higher energies, and O $2p$-Bi $6s$ antibonding bands shift to lower energies.

such an interaction is allowed by symmetry. This can be seen very clearly as the absence and the presence of Bi s states in Bi $6p_{1/2}$ and Bi $6p_{3/2}$ bands in, alternatively, the cubic and the monoclinic phases. Figure 9(b) shows that such hybridization between the O $2p$-Bi $6s$ states and the Bi $6p$ states lowers the energy of occupied O $2p$-Bi $6s$ bands while unoccupied Bi $6p$ states are pushed to higher energy. The asymmetric lattice distortion is favored.

IV. SUMMARY

A-site-ordered cubic perovskite $BiCu_3Cr_4O_{12}$ with mixed-valent $Cr^{+3.75}$ is a paramagnetic metal at room temperature and shows a first-order transition to a ferrimagnetic metal at 190 K, accompanied with a monoclinic structural distortion. The detailed structural analysis indicates that this transition is linked with a charge disproportionation of $Cr^{3.75+}$ into 1:1 ratio of Cr^{4+} and $Cr^{3.5+}$, which itself is triggered by a lone-pair formation of Bi and the resultant asymmetric distortion of the BiO_{12} polyhedra. The asymmetric distortion stabilizes the high-valence state of Cr^{4+} through the formation of a Cr_2O_5 molecular unit, giving rise to the charge ordering. We argue that in the other mixed-valent Cr-ordered perovskite with rare earths, the charge disproportionate state is very likely hidden behind the charge-transferred state. This study shows that, with the help of Bi lone pairs, the hidden charge disproportionation can manifest itself as the ground state. It is tempting to conclude that the introduction of lone-pair effect may be a useful approach in controlling and designing the electronic phase competition in correlated mixed-valent oxides, which is at the heart of correlated electronics.

ACKNOWLEDGMENTS

The authors acknowledge Tomce Runcevski and Milinda Abeykoon for their assistance in the measurement of the synchrotron x-ray diffraction data, Takashi Taniguchi for his support in the high-pressure synthesis, and Ali Bangura for his critical reading of the manuscript. This work was partly supported by Japan Society for the Promotion of Science (JSPS) KAKENHI Grants No. JP24540362, No. JP15H05852, and No. JP17H01140, and Alexander von Humboldt foundation.

[1] D. I. Khomskii, *Transition Metal Compounds* (Cambridge University Press, Cambridge, 2014).
[2] Y. Tokura and N. Nagaosa, Science **288**, 462 (2000).
[3] P. G. Radaelli, D. E. Cox, M. Marezio, and S.-W. Cheong, Phys. Rev. B **55**, 3015 (1997).
[4] T. Ohama, H. Yasuoka, M. Isobe, and Y. Ueda, Phys. Rev. B **59**, 3299 (1999).
[5] C. Urano, M. Nohara, S. Kondo, F. Sakai, H. Takagi, T. Shiraki, and T. Okubo, Phys. Rev. Lett. **85**, 1052 (2000).
[6] J. P. Wright, J. P. Attfield, and P. G. Radaelli, Phys. Rev. Lett. **87**, 266401 (2001).
[7] A. C. Komarek, M. Isobe, J. Hemberger, D. Meier, T. Lorenz, D. Trots, A. Cervellino, M. T. Fernández-Díaz, Y. Ueda, and M. Braden, Phys. Rev. Lett. **107**, 027201 (2011).

[8] T. Toriyama, A. Nakao, Y. Yamaki, H. Nakao, Y. Murakami, K. Hasegawa, M. Isobe, Y. Ueda, A. V. Ushakov, D. I. Khomskii, S. V. Streltsov, T. Konishi, and Y. Ohta, Phys. Rev. Lett. **107**, 266402 (2011).

[9] H. Shiraki, T. Saito, M. Azuma, and Y. Shimakawa, J. Phys. Soc. Jpn. **77**, 064705 (2008).

[10] J. Sanchez-Benitez, J. A. Alonso, M. J. Martinez-Lope, A. Andres, and M. T. Fernandez-Diaz, Inorg. Chem. **49**, 5679 (2010).

[11] S. Zhang, T. Saito, M. Mizumaki, and Y. Shimakawa, Chem. Eur. J. **20**, 9510 (2014).

[12] J. Sugiyama, H. Nozaki, I. Umegaki, E. J. Ansaldo, J. H. Brewer, H. Sakurai, M. Isobe, and H. Takagi, Physics Procedia **75**, 435 (2015).

[13] M. Isobe, H. Sakurai, and H. Takagi, Meet. Abstr. Phys. Soc. Jpn **69**, 386 (2014).

[14] T. Saito, S. Zhang, D. Khalyavin, P. Manuel, J. P. Attfield and Y. Shimakawa, Phys. Rev. B **95**, 041109(R) (2017).

[15] T. Mizokawa, Y. Morita, T. Sudayama, K. Takubo, I. Yamada, M. Azuma, M. Takano, and Y. Shimakawa, Phys. Rev. B **80**, 125105 (2009).

[16] I. Yamada, H. Etani, K. Tsuchida, S. Marukawa, N. Hayashi, T. Kawakami, M. Mizumaki, K. Ohgushi, Y. Kusano, J. Kim, N. Tsuji, R. Takahashi, N. Nishiyama, T. Inoue, T. Irifune, and M. Takano, Inorg. Chem. **52**, 13751 (2013).

[17] A. P. Hammersley, S. O. Svensson, M. Hanfland, A. N. Fitch, and D. Hausermann, High Pressure Res. **14**, 235 (1996).

[18] Bruker AXS. TOPAS, Version 4.2. (Bruker AXS Inc., Madison, WI, 2009).

[19] R. W. Cheary and A. Coelho, J. Appl. Cryst. **25**, 109 (1992).

[20] B. J. Campbell, H. T. Stokes, D. E. Tanner, and D. M. Hatch, J. Appl. Cryst. **39**, 607 (2006).

[21] V. Antonov, B. Harmon, and A. Yaresko, *Electronic Structure and Magneto-optical Properties of Solids* (Kluwer Academic Publishers, Dordrecht/Boston/London, 2004).

[22] See Supplemental Material at http://link.aps.org/supplemental/10.1103/PhysRevB.97.195111 for the detailed structure parameters, the results of ISODISTORT analysis of symmetry modes, and the bond-lengths of Cr2-O in $Cr2O_6$ and Cr3-O in $Cr3O_6$ octahedral.

[23] I. D. Brown and D. Altermatt, J. Acta Crystallogr. B **41**, 244 (1985).

[24] A. Walsh, D. J. Payne, R.G. Egdell, and G.W. Watson, Chem. Soc. Rev. **40**, 4455 (2011).